Data-Driven Gas Sensing Performance of Cu-Doped ZnO Thin Films

Abdul-Lateef Abdul-Jabar[1], Mushtaq Talib Hamzah[1], Rabab Mohammed Habeeb[1], Muhaned Zaidi[2] and Saja Faez Hassan[1]

[1]*Department of Physics, College of Education, Mustansiriyah University, 10052 Baghdad, Iraq*
[2]*Department of Medical Physics, College of Science, Al-Manara University, 62001 Amarah, Iraq*
lateef1991@uomustansiriyah.edu.iq, mushtak1994@uomustansiriyah.edu.iq, muhanedzaidi@uomanara.edu.iq, rabab.m@uomustansiriyah.edu.iq, sajafaez_81@uomustansiriyah.edu.iq

Keywords: ZnO, Copper Doping, Thin Films, CSP, XRD, AFM, Optical Properties, Gas Sensing.

Abstract: This work systematically investigates the effect of Cu doping on the properties of ZnO thin films deposited onto glass substrates via chemical spray pyrolysis (CSP) at 450 °C. A series of undoped films, as well as films doped with 1% and 3% Cu, were synthesized and comprehensively characterized. Structural analysis by XRD verified that all films exhibited a polycrystalline nature with a hexagonal wurtzite structure, demonstrating a growth orientation along the (002) plane. The crystallite size increased from 14.32 nm for ZnO to 25.36 nm (3% Cu), indicating an enhancement in crystallinity. This was supported by a concurrent decrease in dislocation density and microstrain. Atomic force microscopy (AFM) showed that Cu doping significantly reduced surface roughness and average grain size, resulting in smoother and more compact films. Optically, increasing the Cu content resulted in lower visible light transmittance and a higher absorption coefficient. The optical bandgap energy red-shifted from 3.50 eV for ZnO to 3.40 eV for the 3% Cu-doped sample. In gas sensing tests, the 3% Cu-doped film exhibited the highest sensitivity to ammonia (NH_3) due to an increase in electrical resistance. Conversely, sensitivity to hydrogen (H_2) decreased with higher Cu doping levels. The findings conclusively demonstrate that strategic copper doping serves as a controllable method for engineering the properties discussed in this paper, thereby optimizing them for targeted device applications.

1 INTRODUCTION

Zinc oxide (ZnO) continues to attract considerable scientific interest due to its exceptional combination of physicochemical properties, making it an extremely adaptable substance for a wide range of technological uses [1], [2]. Its attractive characteristics include a wide direct bandgap (~3.37 eV [3]), a substantial exciton binding energy (60 meV), and high charge carrier mobility [4]. These inherent properties make ZnO a leading candidate for use in many applications [5]-[10]. Complementing these tunable properties are the material's intrinsic advantages, such as low cost, non-toxicity, and high electron conductivity [11], which further bolster its industrial viability. [12]-[16]. The deliberate engineering of these defects is crucial for enhancing performance in photoelectronic devices, particularly those reliant on efficient light emission. Since the type and concentration of these defects are highly dependent on the fabrication methodology, ZnO thin films have been synthesized using many methods, including magnetron sputtering [17], [18], (MOCVD) [19], sol-gel processing [20], [21], PLD [22], [23], and CSP [24]-[26]. Doping with selective elements represents a primary strategy for further tailoring the functional properties of ZnO, notably its optical and electrical characteristics [27]. The goal of this study is to systematically investigate how the incorporation of Cu affects specific physical characteristics.

2 EXPERIMENTAL

Undoped and ZnO: Cu thin films were synthesized on glass substrates via CSP. The solution was prepared by dissolving 0.05 M of ($Zn(CH_3COO)_2 \cdot 2H_2O$) in 100 mL of deionized water to form the host matrix. Copper doping was accomplished by including ($CuCl_2$) to the precursor solution at concentrations of 1 and 3 at. %, maintaining a doping agent molarity of 0.1 M. The base temperature was fixed at 450 °C throughout the deposition process. To optimize the

film deposition process, the following parameters were maintained: a spraying rate of 0.2 mL per burst, a nozzle-to-base distance of 29 cm, a spray duration of 10 seconds per cycle, an interval of 90 seconds between successive sprays, and a carrier gas (filtered compressed air) pressure of 10^5 Pa. The film thickness, determined by the gravimetric method, was maintained at 330 ± 25 nm. Structural properties were analyzed using XRD. AFM examined surface morphology. Transmittance spectra were recorded using a UV-Vis spectrophotometer. Gas sensing measurements were conducted in a cylindrical chamber with a 10 cm radius and a height of 18 cm.

3 RESULTS AND DISCUSSIONS

Figure 1 presents the X-ray diffraction patterns, where the diffraction peaks corresponding to the (100), (002), (101), and (200) crystal planes show slight shifts from their standard positions at 32.12°, 34.81°, 36.42°, and 63.26°, respectively. The results indicate that the most intense peak is associated with the (002) plane [27], confirming a preferred c-axis orientation. These findings are consistent with the ICDD reference No. 36-1451 and suggest that the incorporation of lithium ions into the zinc oxide lattice slightly modifies the crystal structure, leading to peak shifts while preserving the hexagonal wurtzite phase.

The crystallite size (D) was determined [28], [29] using the standard Scherrer approach. The results show that the peak broadening (β) decreases with increasing copper content up to 3%, which corresponds to an increase in crystallite size from 14.32 to 25.36 nm [30], [31]. This behavior indicates that copper incorporation improves crystallinity, as reduced peak broadening is typically associated with enhanced crystal quality and grain growth.

The dislocation density (δ), calculated using the inverse square of the crystallite size [32], [33], decreases from 35.38 to 20.66 × 10^{14} lines/m², indicating a lower density of structural defects and improved lattice quality [34], [35]. The microstrain (ε), evaluated from peak broadening and diffraction angle [36], [37], decreases from 27.44 to 18.56 × 10^{-4}, suggesting that dopant incorporation helps relieve lattice distortions and stabilize the crystal structure. All calculated structural parameters are summarized in Table 1, while Figure 2 illustrates their variation with copper content.

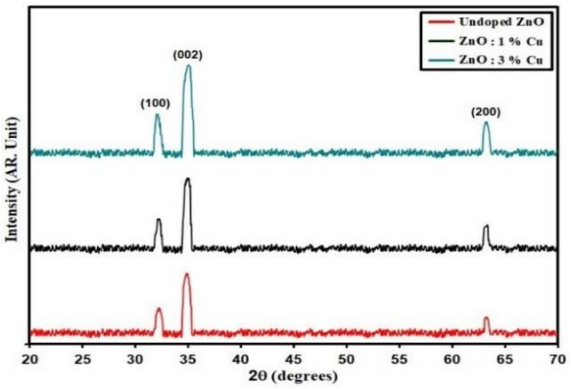

Figure 1: XRD styles of deposit films.

The AFM images presented in Figure 3 provide a detailed visualization of the deposited ZnO films, while Table 2 supplies quantitative data, including average roughness (Ra) and root mean square roughness (Rrms). The images reveal a uniform distribution of microscale granules across the film surfaces, with no visible gaps, as shown in Figures 3 (a_3), 3 (b_3), and 3 (c_3). The calculated average particle size (Pav) decreases systematically with increasing Copper doping, measuring approximately 87.2 nm, 73.9 nm, and 31.8 nm for ZnO, 1% Cu-doped ZnO, and 3% Cu-doped ZnO, respectively [38], [39]. Similarly, the Ra values decline from 9.69 nm for ZnO to 7.40 nm and 4.27 nm for 1% and 3% Cu-doped films, while the Rrms values decrease from 7.84 nm to 5.06 nm and 4.15 nm, respectively. This trend indicates that Copper doping smooths the film surfaces by reducing surface roughness. The reduction in particle size and roughness suggests enhanced film compactness and uniformity [40], [41].

Table 1: *D*, E_g, and structural coefficient of ZnO and ZnO: Cu films.

Specimen	(hkl) Plane	2 θ (°)	FWHM (°)	E_g (eV)	D (nm)	δ (× 10^{14}) (lines/m^2)	ε (× 10^{-4})
ZnO	002	34.81	0.50	3.50	14.32	35.38	27.44
ZnO: 1% Cu	002	34.78	0.48	3.45	22.30	27.79	20.83
ZnO: 3% Cu	002	34.73	0.42	3.40	25.36	20.66	18.56

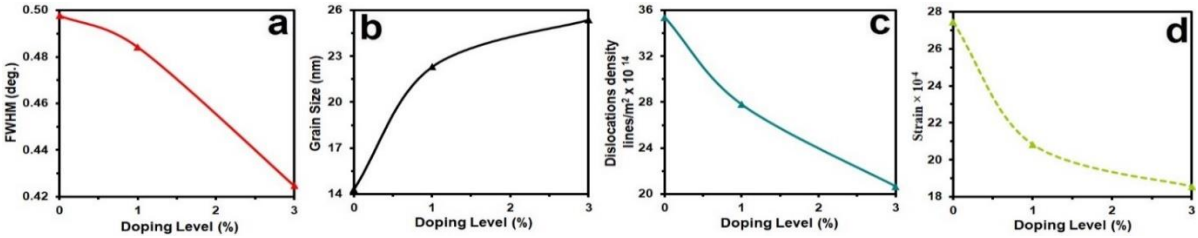

Figure 2: FWHM (a) *D* (b) δ (c) ε (d) for ZnO and ZnO: Cu films.

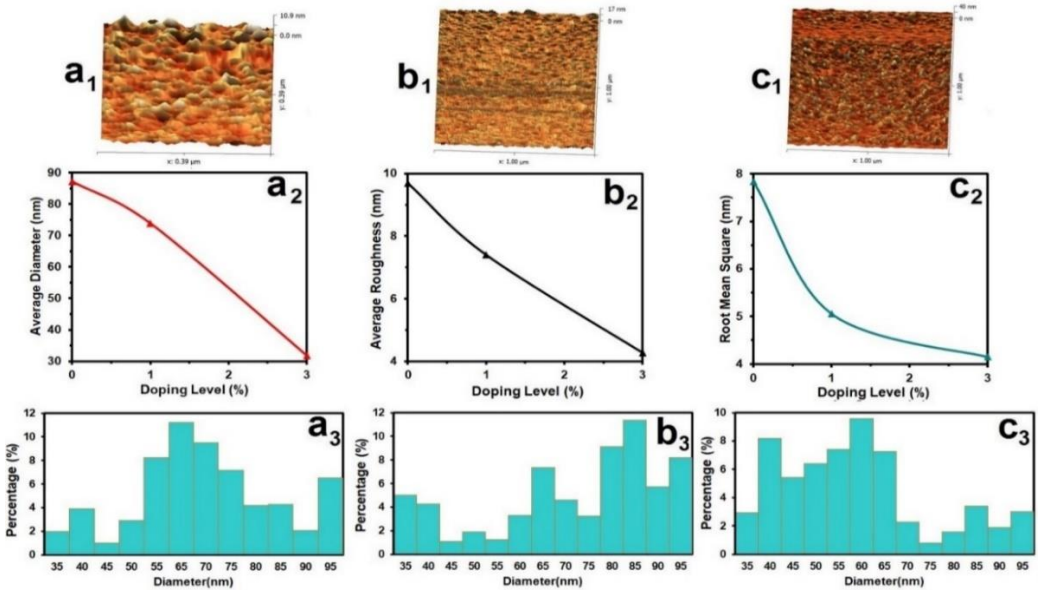

Figure 3: Displays the AFM outcomes for undoped ZnO and ZnO: Cu films.

Table 2: The values of P_{AFM} (parameters obtained from AFM analysis) for the targeted films.

Samples	P_{av} (nm)	R_a (nm)	Rrms (nm)
ZnO	87.2	9.69	7.84
ZnO: 1% Cu	73.9	7.40	5.06
ZnO: 3% Cu	31.8	4.27	4.15

The experimental data are typically expressed in terms of percentage transmittance (T) [42], [43].

$$T\% = \frac{I}{I_o}\%. \quad (1)$$

Where Io and I are the initial light intensity and light intensity after it passes through the sample, respectively, the transmittance of the films, as shown in Figure 4, decreases with increasing copper content. This behavior indicates that the incorporation of copper enhances light absorption within the ZnO films, leading to a reduction in transparency. Additionally, the absorption edge exhibits a red shift as the Cu concentration rises [19]. Figure 5 presents the transition and absorption spectra of the Cu-doped ZnO. From these spectra, it is evident that the transition absorbance values decrease with higher copper doping. Since the transition absorbance is directly related to the optical density of the material, this trend indicates that copper incorporation increases the optical density of the ZnO films, making them more efficient in absorbing incident light [43], [44].

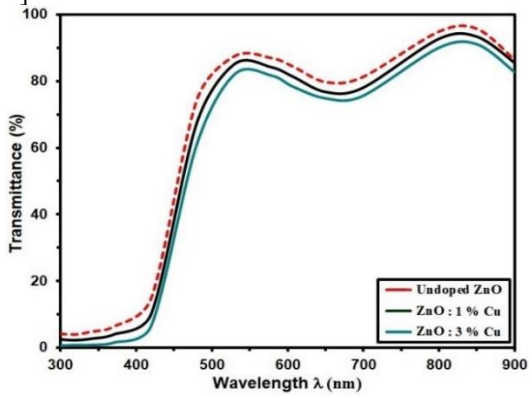

Figure 4: T of the deposit films.

The absorption coefficient (α) was obtained via the following connection [45], [46]:

$$\alpha = (2.303 \times A)/t. \quad (2)$$

Where (t) is film thickness. α, as illustrated in Figure 6, was found to increase with rising copper content. This trend suggests that higher Cu doping enhances the films' ability to absorb incident light, resulting in stronger optical absorption [47], [48].

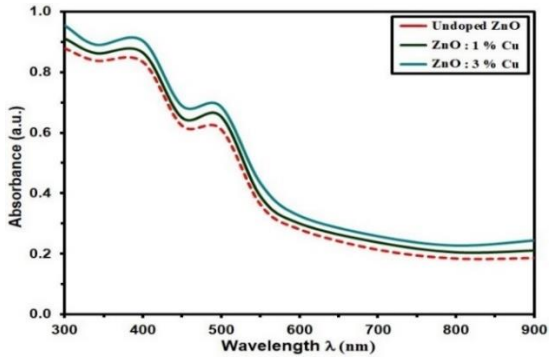

Figure 5: Absorption of deposit films.

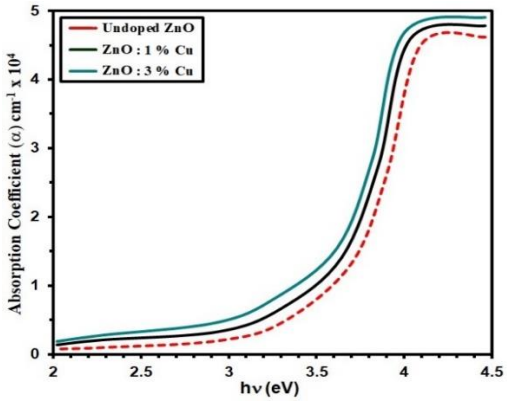

Figure 6: α against wavelength for undoped ZnO and ZnO: Cu films.

Tauc's relation can be utilized to calculate the bandgap energy Eg [49], [50]:

$$(\alpha h\nu) = A\left(h\nu - E_g\right)^{\frac{1}{2}}. \quad (3)$$

In Tauc's relation, A is a constant. Eg was determined from Figure 7. Analysis of the Tauc plots reveals a reduction in E_g from 3.50 eV for ZnO to 3.40 eV with increasing copper content. This bandgap narrowing is related to the introduction of localized states within the band structure due to copper incorporation, which facilitates electronic transitions at lower energies [51], [52].

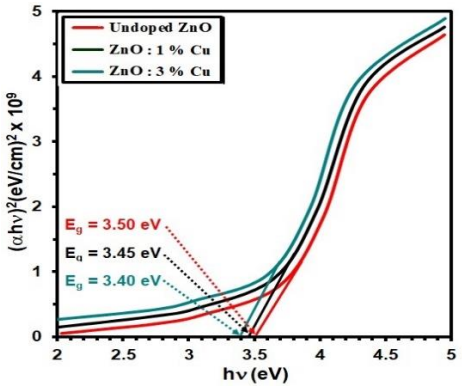

Figure7: Eg for ZnO and ZnO: Cu films.

The extinction coefficient (k) was calculated using (4) [53], [54]:

$$k = \frac{\alpha\lambda}{4\pi}. \quad (4)$$

Figure 7 demonstrates the variation of extinction coefficient (k) via wavelength (λ), showing that k decreases with increasing Cu concentration. This trend suggests that higher Cu doping reduces the optical absorption of the films, resulting in increased transparency [55], [56].

The refractive index (n) is determined via (8) [57], [58]:

$$n = \left(\frac{1+R}{1-R}\right) + \sqrt{\frac{4R}{(1-R)^2} - k^2.} \quad (5)$$

Where R is reflectance. Figure 8 presents a comparative representation of the extinction coefficient (k) for undoped ZnO and ZnO:Cu films Figure 9 illustrates the variation of n with λ. Based on this figure, it is evident that n decreases with increasing Cu content. This reduction in refractive index suggests that Cu incorporation lowers the optical density, likely due to changes in polarizability and a decrease in defect-related electronic states [59], [60].

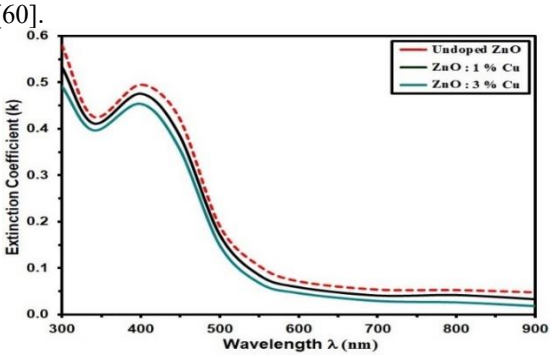

Figure 8: Extinction coefficient (k) for undoped ZnO and ZnO: Cu films.

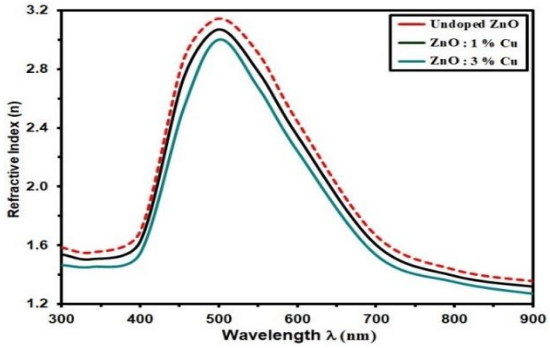

Figure 9: n for ZnO and ZnO: Cu films.

The detection sensitivity, also referred to as the sensor response, was evaluated using a standard relation based on the change in electrical resistance between the gas-exposed and reference states [61], [62].

The gas sensor fabricated from porous silicon coated with zinc oxide on a glass substrate was tested under 270 ppm ammonia at 125°C. Figure 10 shows the resistance–time behavior for both undoped zinc oxide and doped samples. When exposed to ammonia, surface oxidation reactions occur, during which adsorbed oxygen species release trapped electrons back into the conduction band. As a result, the electrical resistance of the zinc oxide film increases, and the potential barrier at grain boundaries becomes higher [63], [64].

Among all investigated samples, the film doped with three percent copper exhibited the highest resistance change, which led to an improved sensor response. This increase in resistance and barrier height indicates that copper doping strengthens the interaction between gas molecules and the film surface, thereby enhancing the overall detection sensitivity [65], [66].

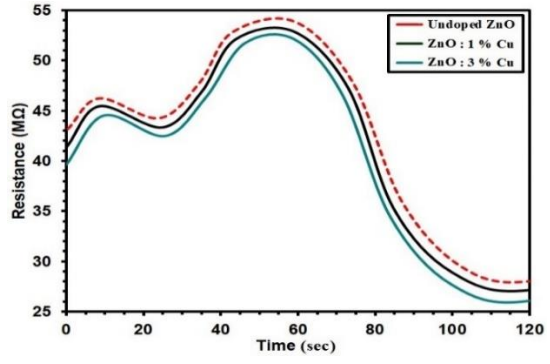

Figure 10: Resistance via operating time for ZnO and ZnO: Cu films.

Figure 11 illustrates that sensitivity to H_2 decreases with increasing Cu doping in ZnO films, due to charge carrier recombination, with ZnO:3 % Cu showing the lowest sensitivity [67, 68]. For different doping levels, undoped ZnO, ZnO: 1% Cu, and ZnO: 3% Cu, sensitivity decreased from 41.26% to 16.38% at 90 ppm, from 42.61% to 7.58% at 180 ppm, and from 44.20% to 18.93% at 270 ppm [67], [68]. The reduction in sensitivity for ZnO, ZnO: 2% Cu, and ZnO: 4% Cu indicates that higher Cu doping levels result in decreased sensor responsiveness to NH_3 gas [69], [70].

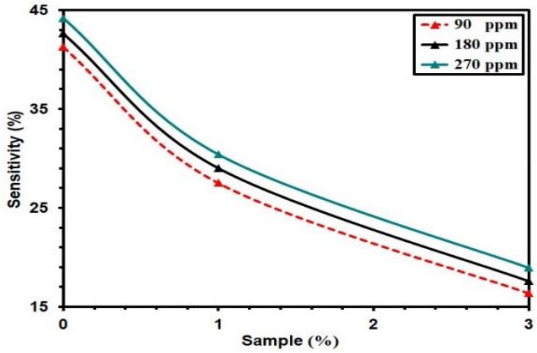

Figure 11: Sensitivity of ZnO and ZnO:Cu films.

4 CONCLUSIONS

This study successfully fabricated undoped and copper-doped ZnO thin films (1% and 3% Cu) via CSP. XRD confirmed the polycrystalline nature of all films, revealing a hexagonal wurtzite structure with a predominant (002) plane orientation. The incorporation of Cu into the ZnO lattice resulted in an increase in crystallite size from 14.32 nm to 25.36 nm, accompanied by a corresponding decrease in dislocation density and microstrain, indicating a significant enhancement in the crystallinity and structural quality of the films. Morphological studies via atomic force microscopy revealed that Cu doping effectively reduced the average surface roughness and grain size, resulting in smoother and more compact films. Optically, the doped films exhibited a decrease in transmittance and a red shift in the absorption edge, accompanied by an increase in the absorption coefficient. The optical bandgap energy exhibited a redshift, decreasing from 3.50 eV for undoped ZnO to 3.40 eV for the 3% Cu-doped sample. This reduction is related to the introduction of defect energy levels within the band structure, facilitated by Cu incorporation. Gas sensing performance evaluation revealed that the 3% Cu-

doped ZnO film exhibited the highest sensitivity towards ammonia (NH_3), attributed to an enhanced surface reaction and reduced electrical resistance. Conversely, sensitivity to hydrogen (H_2) decreased with higher Cu concentration.

ACKNOWLEDGMENTS

The research was made possible by Mustansiriyah University (www.uomustansiriyah.edu.iq), for which the authors are incredibly thankful.

REFERENCES

[1] P. Rong, S. Ren, and Q. Yu, "Fabrications and applications of ZnO nanomaterials in flexible functional devices—A review," Critical Reviews in Analytical Chemistry, vol. 49, no. 4, pp. 336-349, 2019.

[2] G. Hu, S. Q. Li, H. Gong, Y. Zhao, J. Zhang, T. L. S. L. Wijesinghe, et al., "White light from an indium zinc oxide/porous silicon light-emitting diode," Journal of Physical Chemistry C, vol. 113, pp. 751-754, 2009.

[3] J. Wienke, B. van der Zanden, M. Tijssen, and M. Zeman, "Performance of spray-deposited ZnO:In layers as front electrodes in thin-film silicon solar cells," Solar Energy Materials and Solar Cells, vol. 92, pp. 884-890, 2008.

[4] M. Ahmad, J. Zhao, J. Iqbal, W. Miao, L. Xie, R. Mo, and J. Zhu, "Conductivity enhancement by slight indium doping in ZnO nanowires for optoelectronic applications," Journal of Physics D: Applied Physics, vol. 42, no. 16, p. 165406, 2009.

[5] Z. C. Feng, Handbook of Zinc Oxide and Related Materials: Volume One, CRC Press, 2013.

[6] A. Mang and K. Reimann, "Band gaps, crystal-field splitting, spin-orbit coupling, and exciton binding energies in ZnO under hydrostatic pressure," Solid State Communications, vol. 94, no. 4, pp. 251-254, 1995.

[7] Janotti and C. G. Van de Walle, "Fundamentals of zinc oxide as a semiconductor," Reports on Progress in Physics, vol. 72, no. 12, p. 126501, 2009.

[8] K. Ellmer and R. Mientus, "Carrier transport in polycrystalline transparent conductive oxides: A comparative study of zinc oxide and indium oxide," Thin Solid Films, vol. 516, no. 14, pp. 4620-4627, 2008.

[9] Z. Zhu, B. Li, J. Wen, Z. Chen, and Z. Chen, et al., "Indium-doped ZnO horizontal nanorods for high on-current field effect transistors," RSC Advances, vol. 7, no. 87, pp. 54928-54933, 2017.

[10] M. Kumar, L. Wen, B. B. Sahu, and J. G. Han, "Simultaneous enhancement of carrier mobility and concentration via tailoring of Al-chemical states in Al-ZnO thin films," Applied Physics Letters, vol. 106, p. 241903, 2015.

[11] S. Dutta, S. Chattopadhyay, A. Sarkar, M. Chakrabarti, D. Sanyal, and D. Jana, "Role of defects in tailoring structural, electrical and optical properties of ZnO," Progress in Materials Science, vol. 54, no. 1, pp. 89-136, 2009.

[12] J. A. Sans, J. F. Sánchez-Royo, A. Segura, G. Tobias, and E. Canadell, "Chemical effects on the optical band-gap of heavily doped ZnO," Physical Review B, vol. 79, no. 19, p. 195105, 2009.

[13] K. Djessas, I. Bouchama, J. L. Gauffier, and Z. B. Ayadi, "Effects of indium concentration on the properties of In-doped ZnO films," Thin Solid Films, vol. 555, pp. 28-32, 2014.

[14] A. Hafdallah, F. Yanineb, M. S. Aida, and N. Attaf, "In doped ZnO thin films," Journal of Alloys and Compounds, vol. 509, no. 26, pp. 7267-7270, 2011.

[15] E. S. Babu and S. K. Hong, "Effect of indium concentration on morphology of ZnO nanostructures grown by CVD and their application for H2 gas sensing," Superlattices and Microstructures, vol. 82, pp. 349-356, 2015.

[16] S. Hong, H. H. Park, J. Moon, and H. H. Park, "Effect of metal dopants on ZnO thin films," Thin Solid Films, vol. 515, no. 3, pp. 957-960, 2006.

[17] Huang, M. Wang, Z. Deng, Y. Cao, et al., "Low content indium-doped zinc oxide films with tunable work function," Semiconductor Science and Technology, vol. 25, no. 4, p. 045008, 2010.

[18] M. Girtan, M. Kompitsas, R. Mallet, and I. Fasaki, "On physical properties of doped ZnO films on PET substrates," European Physical Journal Applied Physics, vol. 51, no. 3, 2010.

[19] R. Bel-Hadj-Tahar and A. B. Mohamed, "Sol-gel processed indium-doped zinc oxide thin films," New Journal of Glass and Ceramics, vol. 4, no. 4, p. 55, 2014.

[20] K. Matsubara, P. Fons, K. Iwata, A. Yamada, et al., "ZnO transparent conducting films deposited by PLD," Thin Solid Films, vol. 431-432, pp. 369-372, 2003.

[21] S. R. Ardekani, A. S. R. Aghdam, M. Nazari, A. Bayat, E. Yazdani, and E. Saievar-Iranizad, "A comprehensive review on ultrasonic spray pyrolysis technique," Journal of Analytical and Applied Pyrolysis, p. 104631, 2019.

[22] G. Singh, S. B. Shrivastava, D. Jain, et al., "Effect of indium doping on ZnO films," Bulletin of Materials Science, vol. 33, pp. 581-587, 2010.

[23] C. Hsu, C. C. Tsao, Y. H. Chen, and X. Z. Zhang, "Bipolar resistive switching characteristics of a sol-gel InZnO oxide semiconductor," Physica B: Condensed Matter, vol. 561, pp. 64-69, 2019.

[24] C. Falcony, M. A. Aguilar-Frutis, and M. García-Hipólito, "Spray pyrolysis technique; high-K dielectric films and luminescent materials: a review," Micromachines, vol. 9, no. 8, p. 414, 2018.

[25] A. Chakraborty, T. Mondal, S. K. Bera, S. K. Sen, R. Ghosh, and G. K. Paul, "Effects of aluminum and indium incorporation on the structural and optical properties of ZnO thin films synthesized by spray pyrolysis technique," Materials Chemistry and Physics, vol. 112, no. 1, pp. 162-166, 2008.

[26] B. Djurišić, Y. H. Leung, K. H. Tam, Y. F. Hsu, et al., "Defect emissions in ZnO nanostructures," Nanotechnology, vol. 18, no. 9, p. 095702, 2007.

[27] K. U. Sim, S. W. Shin, A. V. Moholkar, J. H. Yun, J. H. Moon, and J. H. Kim, "Effects of dopant on the characteristics of ZnO thin films prepared by RF magnetron sputtering," Current Applied Physics, vol. 10, no. 3, pp. S463-S467, 2010.

[28] K. Ramamoorthy, K. Kumar, R. Chandramohan, and K. Sankaranarayanan, "Review on material properties of IZO thin films useful as epi-n-TCOs," Materials Science and Engineering B, vol. 126, no. 1, pp. 1-15, 2006.

[29] R. S. Ali, H. S. Rasheed, N. F. Habubi, and S. S. Chiad, "Synthesis and characterization of manganese-doped FeS2 thin films via chemical spray pyrolysis," Chalcogenide Letters, vol. 20, no. 1, pp. 63-72, 2023.

[30] M. Shaheera, K. G. Girija, M. Kaur, et al., "Characterization and device application of indium doped ZnO homojunction prepared by RF magnetron sputtering," Optical Materials, vol. 101, p. 109723, 2020.

[31] S. Y. Lim, S. Brahma, C. P. Liu, R. C. Wang, and J. L. Huang, "Effect of indium concentration on luminescence and electrical properties of indium doped ZnO nanowires," Thin Solid Films, vol. 549, pp. 165-171, 2013.

[32] M. Caglar, S. Ilican, and Y. Caglar, "Influence of dopant concentration on the optical properties of ZnO:In films by sol-gel method," Thin Solid Films, vol. 517, no. 17, pp. 5023-5028, 2009.

[33] A. Bader, S. K. Muhammad, A. M. Jabbar, K. H. Abass, S. S. Chiad, and N. F. Habubi, "Synthesis and characterization of indium-doped CdO nanostructured thin films," Journal of Nanostructures, vol. 10, no. 4, pp. 744-750, 2020.

[34] W. A. Aelawi, S. Alptekin, and M. H. Al-Timimi, "Structural, optical, and electrical properties of nanocrystalline CdS1−xCuxS thin films," Indian Journal of Physics, vol. 97, no. 13, pp. 3949-3956, 2023.

[35] S. Mourad, J. E. Ghoul, and K. Khirouni, "Role of indium doping on structural and electrical properties of ZnO nanoparticles prepared by sol-gel method," Journal of Materials Science: Materials in Electronics, vol. 31, pp. 6372-6384, 2020.

[36] R. Yousefi, F. Jamali-Sheini, A. K. Zak, and M. R. Mahmoudian, "Effect of indium concentration on morphology and optical properties of In-doped ZnO nanostructures," Ceramics International, vol. 38, no. 8, pp. 6295-6301, 2012.

[37] K. J. Chen, F. Y. Hung, S. J. Chang, and Z. S. Hu, "Microstructures, optical and electrical properties of In-doped ZnO thin films prepared by sol-gel method," Applied Surface Science, vol. 255, no. 12, pp. 6308-6312, 2009.

[38] A. S. Al Rawas, M. Y. Slewa, B. A. Bader, N. F. Habubi, and S. S. Chiad, "Physical characterization of nickel doped nanostructured TiO2 thin films," Journal of Green Engineering, vol. 10, no. 9, pp. 7141-7153, 2020.

[39] B. Zhang, D. Xiong, S. Xu, W. Ouyang, et al., "Highly efficient field emission from indium-doped ZnO nanostructure," Materials Letters, vol. 222, pp. 25-28, 2018.

[40] C. Yu, R. Li, T. Li, H. Dong, W. Jia, and B. Xu, "Effect of indium doping on photoelectric properties of ZnO nanorods/GaN LEDs," Superlattices and Microstructures, vol. 120, pp. 298-304, 2018.

[41] K. H. Tam, C. K. Cheung, Y. H. Leung, A. B. Djurišić, C. C. Ling, et al., "Defects in ZnO nanorods prepared by hydrothermal method," Journal of Physical Chemistry B, pp. 20865-20871, 2006.

[42] H. Hadi, M. A. Abbas, A. A. Khadayeir, Z. M. Abood, N. F. Habubi, and S. S. Chiad, "Effects of Mn doping on TiO2 thin films," Journal of Physics: Conference Series, vol. 1664, no. 1, 2020.

[43] A. A. Kamil, N. A. Bakr, T. H. Mubarak, and J. Al-Zanqanawee, "Synthesis and study of Au and Ag nanoparticles by PLAL technique," Digest Journal of Nanomaterials and Biostructures, vol. 16, no. 4, pp. 1219-1226, 2021.

[44] C. H. Ahn, Y. Y. Kim, D. C. Kim, S. K. Mohanta, and H. K. Cho, "A comparative analysis of deep level emission in ZnO layers," Journal of Applied Physics, vol. 105, no. 1, p. 013502, 2009.

[45] B. A. Ibrahem, A. M. A. Karim, and T. H. Mubarak, "Study of the effect of cobalt on nickel ferrite properties," Materials Today: Proceedings, 2023.

[46] S. K. Muhammad, E. S. Hassan, K. Y. Qader, K. H. Abass, S. S. Chiad, and N. F. Habubi, "Effect of vanadium on structure and morphology of SnO2 thin films," Nano Biomedicine and Engineering, vol. 12, no. 1, pp. 67-74, 2020.

[47] Chandrinou, N. Boukos, C. Stogios, and A. Travlos, "PL study of oxygen defect formation in ZnO nanorods," Microelectronics Journal, vol. 40, no. 2, pp. 296-298, 2009.

[48] Y. R. Denny, H. C. Shin, S. Seo, S. K. Oh, et al., "Electronic and optical properties of Hf-In-Zn-O thin film," Journal of Electron Spectroscopy and Related Phenomena, vol. 185, no. 1-2, pp. 18-22, 2012.

[49] C. Park, S. M. Hwang, J. H. Choi, Y. H. Kwon, et al., "Effects of In or Ga doping on ZnO nanorods," Physica Status Solidi A, vol. 210, no. 8, pp. 1552-1556, 2013.

[50] A. Hussin, R. S. Al-Hasnawy, R. I. Jasim, N. F. Habubi, and S. S. Chiad, "Optical and structural properties of Mn-doped CuO thin films," Journal of Green Engineering, vol. 10, no. 9, pp. 7018-7028, 2020.

[51] J. F. Moulder, W. F. Stickle, P. E. Sobol, and K. D. Bomben, Handbook of X-ray Photoelectron Spectroscopy, Perkin-Elmer Corporation, 1992.

[52] K. Hamaida, M. Bouslama, M. Ghaffour, F. Besahraoui, et al., "Growth of In2O3 by electron irradiation," Surface Review and Letters, vol. 19, no. 6, p. 1250066, 2012.

[53] A. Teke, Ü. Özgür, S. Doğan, X. Gu, H. Morkoç, B. Nemeth, et al., "Excitonic fine structure in ZnO," Physical Review B, vol. 70, no. 19, p. 195207, 2004.

[54] Zeng, G. Duan, Y. Li, S. Yang, X. Xu, and W. Cai, "Blue luminescence of ZnO nanoparticles," Advanced Functional Materials, vol. 20, pp. 561-572, 2010.

[55] F. Kayaci, S. Vempati, I. Donmez, N. Biyikli, and T. Uyar, "Role of defects in ZnO photocatalysis," Nanoscale, vol. 6, pp. 10224-10234, 2014.

[56] Ü. Özgür, Y. I. Alivov, C. Liu, A. Teke, M. A. Reshchikov, S. Doğan, and H. Morkoç, "A comprehensive review of ZnO materials and devices," Journal of Applied Physics, vol. 98, no. 4, 2005.

[57] S. Pati, P. Banerji, and S. B. Majumder, "Properties of indium doped ZnO thin films," RSC Advances, vol. 5, no. 75, pp. 61230-61238, 2015.

[58] M. Shaker, R. R. Ahmed, A. M. Mohammad, T. H. Mubarak, and I. H. Mohamed, "Synthesis of CoZnFe2O4 nanoparticles for biomedical applications," Passer Journal of Basic and Applied Sciences, vol. 6, no. 2, pp. 488-493, 2024.

[59] S. Vempati, J. Mitra, and P. Dawson, "One-step synthesis of ZnO nanosheets," Nanoscale Research Letters, vol. 7, no. 1, p. 470, 2012.

[60] C. C. Singh and E. Panda, "Zinc interstitial threshold in Al-doped ZnO film," Journal of Applied Physics, vol. 123, p. 165106, 2018.

[61] S. Hassan, A. K. Elttayef, S. H. Mostafa, M. H. Salim, and S. S. Chiad, "Silver oxide nanoparticles in gas sensor applications," Journal of Materials Science: Materials in Electronics, vol. 30, no. 17, pp. 15943-15951, 2019.

[62] Stavale, N. Nilius, and H. J. Freund, "STM luminescence spectroscopy of intrinsic defects in ZnO thin films," Journal of Physical Chemistry Letters, vol. 4, no. 22, pp. 3972-3976, 2013.

[63] P. Bappaditya, D. Sarkar, and P. K. Giri, "Structural, optical, and magnetic properties of Ni-doped ZnO nanoparticles," Applied Surface Science, vol. 356, pp. 804-811, 2015.

[64] A. B. Djurišić, X. Chen, Y. H. Leung, and A. M. C. Ng, "ZnO nanostructures: growth, properties and applications," Journal of Materials Chemistry, vol. 22, no. 14, pp. 6526-6535, 2012.

[65] B. Djurišić, A. M. C. Ng, and X. Y. Chen, "ZnO nanostructures for optoelectronics," Progress in Quantum Electronics, vol. 34, no. 4, pp. 191-259, 2010.

[66] B. Djurišić and Y. H. Leung, "Optical properties of ZnO nanostructures," Small, vol. 2, no. 8-9, pp. 944-961, 2006.

[67] Singh, S. Chaudhary, and D. K. Pandya, "High conductivity indium doped ZnO films by co-sputtering," Acta Materialia, vol. 111, pp. 1-9, 2016.

[68] M. Girtan, M. Socol, B. Pattier, M. Sylla, and A. Stanculescu, "Properties of sol-gel deposited ZnO:In films," Thin Solid Films, vol. 519, no. 2, pp. 573-577, 2010.

[69] M. N. Jung, E. S. Lee, T. I. Jeon, et al., "Extrinsic carrier concentration of indium doped ZnO tetrapods," Journal of Alloys and Compounds, vol. 481, no. 1-2, pp. 649-653, 2009.

[70] Y. Xu, B. Bo, X. Gao, and Z. Qiao, "Passivation effect on ZnO films by SF6 plasma treatment," Crystals, vol. 9, no. 5, p. 236, 2019.